Transient Hole Burning and Solvation Dynamics of Chlorophyll *b* Monomers in Various Solvent Environments

Jari A. I. Oksanen,*,† Peter Martinsson,‡ Eva Åkesson,‡ Paavo H. Hynninen,§ and Villy Sundström*,‡

Department of Physical Chemistry, University of Jyväskylä, P.O. Box 35, FIN-40351 Jyväskylä, Finland; Department of Chemical Physics, Lund University, P.O. Box 124, S-22100, Lund, Sweden; and Department of Chemistry, University of Helsinki, P.O. Box 55, FIN-00014, University of Helsinki, Finland

Received: November 18, 1997; In Final Form: February 20, 1998

We present a femtosecond transient absorption study of chlorophyll *b* monomers in various solvent environments. Transient absorption spectra and kinetics of chlorophyll *b* were measured in neat pyridine and acetone. The kinetics were measured also for three samples of chlorophyll *b* dissolved in 3-methylpentane and titrated with pyridine. Characteristic for all chlorophyll *b* samples is a very strong excited-state absorption, which significantly affects time-resolved anisotropy values in the wavelength region of our study (600−750 nm). The excited-state absorption spectrum was simulated, and on the basis of time-resolved anisotropy measurements the broad and smooth excited-state absorption band was found to be composed of several transitions to higher excited states. For all of the chlorophyll *b* samples studied, we observed two fast lifetime components (∼100 fs and 1−3 ps). The former component is assigned to transient hole burning of the inhomogeneously broadened ground-state absorption spectrum, while the latter component, which is sensitive to properties of the solvent, is suggested to arise mainly from solvent relaxation.

Introduction

The rate of energy equilibration and flow in photosynthetic antenna complexes have been extensively studied using recent developments of ultrafast lasers and time-resolved spectroscopy in the femtosecond time domain.[1,2] The detailed construction and the pigment composition of the antennae vary in different types of photosynthetic organisms (purple bacteria, green bacteria, green plants, algae, etc.). Despite the dissimilarities in antenna structures, all the light-harvesting complexes are characterized by rapid energy transfer and equilibration among the pigment molecules and very high efficiency of energy-to-charge conversion.

The most abundant light-harvesting complex is the LHC II complex of green plants. It is associated with photosystem II and contains both chlorophyll *a* (Chl *a*) and chlorophyll *b* (Chl *b*).[3] Owing to their diverse molecular structures (Figure 1), the two plant chlorophylls absorb light at different wavelengths. Absorption maxima of the lowest energy electronic transition (Q_y) of monomeric Chl *b* and Chl *a* in diethyl ether lie at 642 and 660 nm, respectively.[4,5] In the light-harvesting process, both pigments are responsible for the capture of light energy. The absorption of light by Chl *b* is followed by a rapid energy transfer to Chl *a*. This fundamental energy transfer step has been studied by several groups applying different types of spectroscopic methods. Fluorescence upconversion measurements on LHC II resolved a lifetime in the subpicosecond region and a second lifetime of several picoseconds.[6,7] Both lifetimes were assigned to energy transfer between differently coupled pigments in the LHC II antenna. Isotropic transient absorption studies yielded similar lifetimes; Bittner et al.[8] excited the LHC II complex near the Chl *b* absorption maximum (645 nm) and monitored the transient absorption kinetics at 655 nm. The decay consisted of contributions from photobleaching (PB) and stimulated emission (SE) during the first 20 ps. Chl *b*-to-Chl *a* energy transfer was again concluded to be subpicosecond. At longer times the absorption difference signal turned into a positive one, and the phenomenon was concluded to arise from excited-state absorption (ESA). Similar positive absorption difference signals at long delay times were observed in other

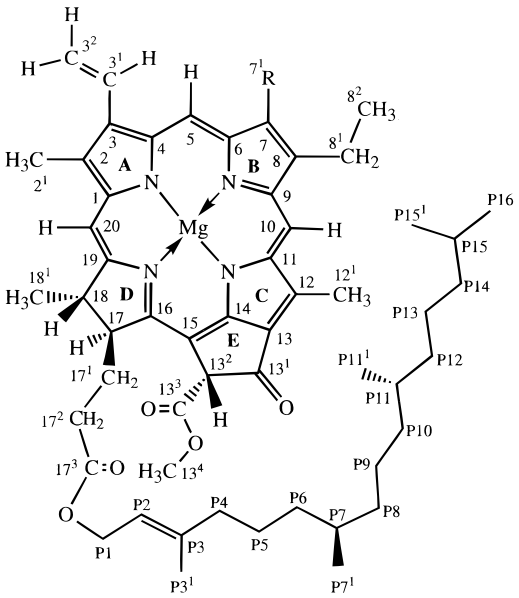

Figure 1. Structures and numbering system of chlorophyll *a* and chlorophyll *b*. Chl *a*: R = CH_3 (methyl); Chl *b*: R = CHO (formyl).

* To whom correspondence should be addressed.
† University of Jyväskylä.
‡ Lund University.
§ University of Helsinki.

S1089-5639(98)00252-7 CCC: $15.00
Published on Web 04/22/1998

studies, when Chl *b* was selectively excited around 645 nm and the LHC II preparation was probed at 650−670 nm.[9,10]

Measurements of transient absorption anisotropy is a method widely used to investigate intermolecular energy transfer. Using linearly polarized excitation and probe pulses, the initial anisotropy value before any depolarization occurs is 0.4, when only ground-state (S_0) bleaching and stimulated emission of the first excited state (S_1) are detected. Pålsson et al.[11] studied the single-color anisotropy decays of the LHC II complex at 650 and 665 nm. The anisotropy decayed to a constant value 0.2 in less than 1 ps. However, a low initial anisotropy value of 0.3 was recorded, and the authors concluded that a very fast initial decay of the anisotropy was not fully resolved in their experiment. The one-color transient absorption study by Kwa et al.[12] detected a strong ESA in the wavelength range 640−660 nm. Furthermore, the anisotropy measurements could not resolve any anisotropy in that region. They inferred that the depolarization was much faster than the time resolution of their experimental setup. At longer wavelengths (665−675 nm), a decaying anisotropy with a time constant of 5 ps was evident, but the initial anisotropy was still far from the theoretical maximum value of 0.4 in their experiments. In a more recent study by Savikhin et al.,[13] anisotropy decay times identical to those of Kwa et al.[12] were obtained in the long wavelength range, but higher values for the initial anisotropy (0.32−0.34) were observed. In some transient absorption studies of LHC II, initial anisotropy values even larger than 0.4 have been measured.[14]

Here we present a femtosecond transient absorption study of Chl *b* monomers in different solvents and solvent mixtures. The spectroscopic characterization of monomeric Chl *b* is essential for the interpretation of the energy-transfer studies, where Chl *b* is involved. We believe it is important to find an explanation for the varying anisotropy values that have been reported for LHC II by several groups. In this contribution, the isotropic and anisotropic absorption difference profiles are measured at different probe wavelengths after the Q_y band of Chl *b* is excited. Transient absorption spectra of Chl *b* in neat pyridine are recorded over a broad wavelength range at various delay times and at four different excitation wavelengths. The excited-state absorption of monomeric Chl *b* was found to give a strong contribution to the spectrum over the entire wavelength region studied (600−750 nm). The initial anisotropy values vary strongly as a function of probing wavelength due to ESA having a polarization different from that of PB and SE. The time evolution of the transient absorption spectrum and kinetics measured at specific wavelengths in different solvents and solvent mixtures are discussed in terms of transient hole burning in the ground-state absorption spectrum, solvent relaxation processes, and vibrational relaxation. As a conclusion, our results show that the excited-state absorption of Chl *b* may play a significant role for the interpretation of isotropic and anisotropic transient absorption results of light-harvesting complexes containing Chl *b* and that monomeric Chl *b* exhibits ultrafast dynamics in ground and excited states following excitation by a femtosecond pulse.

Materials and Methods

A modification (Hynninen, P. H., unpublished work) of a previously published method[15] was used for the preparation of anhydrous Chl *b*. The UV/vis and ^{1}H NMR spectroscopic characteristics agreed with the data obtained previously.[5] The aliphatic hydrocarbon solvent 3-methylpentane (3-MP) (Acros, >99%) was dried with activated aluminum oxide, and it was stored over 4 Å molecular sieves. No drying procedures were applied for the polar solvents acetone and pyridine (Merck, >99.5%). The absorption spectrum of Chl *b* in neat 3-MP shows the maximum absorption of the Q_y band at 645 nm. In acetone and pyridine, the Q_y band maxima are positioned at 645 and 655 nm, respectively.

In the titration experiments, polar (nucleophilic) ligands were added to the neat Chl *b*/3-MP solution with a microliter syringe to achieve the required Chl *b*/ligand molar ratio. The extent of pigment−ligand complexes versus self-aggregated species in the sample preparation was determined from the electronic absorption spectrum. The nominal pigment molarity in the samples was adjusted to 5×10^{-5} mol/L. Solid Chl *b* dissolves slowly in 3-MP, and thus the process was accelerated by mild sonication. A Jasco V-530 UV/vis spectrophotometer was used to record the absorption spectra of titrated samples in quartz cuvettes with a path length of 2 mm. For the simulation of the ESA spectrum, the emission spectrum of Chl *b* in neat pyridine was scanned with a Spex 1681 fluorescence spectrometer in a 10 mm path length quartz cuvette, and the absorption spectrum was measured in the same cuvette. A Chl *b* concentration in the range of 5×10^{-6}−1×10^{-5} mol/L was used for these measurements. Fresh samples were prepared frequently to avoid a presence of the prime derivative of Chl *b*.[16]

A femtosecond two-color transient absorption setup was used in the time-resolved experiments. An argon ion laser (Beam-Lok, Spectra Physics) pumped Ti:sapphire laser (Tsunami, Spectra Physics) generated 100 fs seed pulses at 800 nm at a repetition rate of 82 MHz and a pulse energy of 12 nJ. The seed pulses were stretched and then amplified inside a Nd:YLF (Merlin, Spectra Physics) pumped Ti:sapphire amplifier (Spitfire, Spectra Physics). After amplification the pulses were compressed, yielding 70 fs pulses with a pulse energy of 0.36 mJ at a repetition rate of 5 kHz. A beam splitter was used to split off a part of the output beam for white light continuum generation in a sapphire plate. The probing wavelengths were selected from the continuum with a monochromator placed after the sample. The rest of the beam was directed to seed a travelling wave parametric oscillator (Topas, Light Conversion Ltd.) for generation of a broad range of excitation wavelengths.

Glan polarizers were placed in both pump and probe beams, and a Berek compensator was used in the excitation beam to change the angle between pump and probe polarizations for anisotropy measurements. To minimize interference of photoproducts and sample degradation with the transient absorption signal, the kinetics were measured in a rotating sample cell. The cell was a hollow quartz disk, which was filled with the sample and rotated by a motor at a speed of ∼50 rounds/s, ensuring complete replacement of the sample volume between two successive excitation pulses. The path length of the rotating cell was 2 mm, and the Chl *b* absorbance at the Q_y band maximum was adjusted to 0.4−0.8. The excitation intensity was set to 4×10^{14} photons pulse^{-1} cm^{-2}.

The detection system consisted of three photodiodes. One photodiode measured the intensity fluctuations of the excitation light, and data points where the excitation intensity deviated considerably from its mean value were rejected. Another photodiode detected the probe light, and a third photodiode measured the intensity of the reference beam (interaction with the sample without pump light). The construction of the three-diode system and the optical setup is described in detail elsewhere.[17] Transient absorption kinetics (ΔA versus time) and transient absorption spectra (ΔA versus wavelength at a fixed delay time between the excitation and probe pulses) were

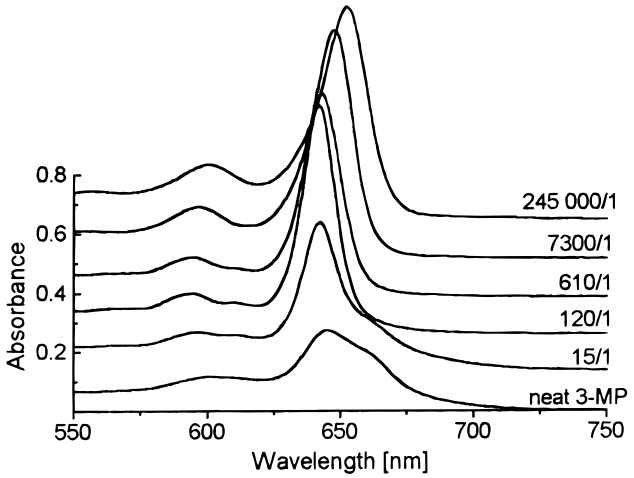

Figure 2. Titration of Chl *b* in 3-methylpentane with pyridine. The Q_y region of the absorption spectrum is plotted. Digits denote molar ratios of pyridine/Chl *b* in the samples.

measured with the same setup. To obtain accurate zero delay time positions at all wavelengths in measurements of transient absorption spectra, the dispersion curve of the setup was determined. When the transient absorption spectrum of a sample was measured, the delay line was simultaneously moved according to this dispersion curve to correct for the dispersion of the detection system. Measured kinetics were analyzed with a deconvolution software (Spectra, Institute of Physics of Estonian Academy of Science, Tartu, 1993). The width of the apparatus response function of the measurement system was 130 fs. All measurements were performed at room temperature.

Results

The absorption spectrum of Chl *b* in neat 3-MP is shown in Figure 2; in addition to the Q_y absorption maximum at 645 nm, there is a red-shifted shoulder due to self-aggregated Chl *b* of various aggregation numbers.[18,19] The addition of pyridine or acetone to the self-aggregated Chl *b* sample readily dissociates the aggregates producing pigment−ligand monomeric species.[20] This is a consequence of the strong interaction of the polar ligand with the central magnesium atom of Chl *b*, preventing entirely the Chl *b*−Chl *b* interactions.[21] Already at a pyridine/Chl *b* molar ratio of 15/1, noticeable changes in the Q_y region of the absorption spectrum are induced (Figure 2). The ligand/pigment molar ratios in 3-MP solution and the corresponding wavelength maxima are listed in Table 1. At a pyridine/Chl *b* molar ratio of 120/1, the red-shifted shoulder in the spectrum of the self-aggregate vanished, and only pigment−pyridine monomeric complexes were present, giving rise to the symmetric Q_y absorption band centered at 642 nm. In the sample with *n*(pyridine)/*n*(Chl *b*) = 120/1, the number of solvent (3-MP) molecules is more than 1000 times larger than that of the ligand (pyridine) molecules, which leaves the dielectric properties of the 3-MP bulk solvent basically unaltered. High pyridine concentrations have an influence on the position of the Q_y band maximum, red-shifting the Q_y band with an onset at a pyridine/Chl *b* molar ratio of 610/1. For higher pyridine concentrations, the Q_y band red shifts gradually with increasing pyridine molarity and reaches the λ_{max} value of 655 nm in neat pyridine. Titration of Chl *b* in 3-MP with acetone is characterized by a markedly weaker tendency of the ligand to attach to the central magnesium atom (Figure 3). Compared to pyridine, a 100-fold higher concentration of acetone is required to prevent self-aggregation of Chl *b* (acetone/Chl *b* molar ratio ∼ 10 000/1). A similar difference between the ligation tendency of pyridine and acetone has been observed for the ligand-induced disaggregation of Chl *a* dimers in carbon tetrachloride.[22] At very high acetone concentrations, the position of the Q_y band maximum also red shifts, but the influence of the acetone concentration on the Q_y band shift is not as pronounced as in the case of pyridine. The Q_y band maximum at an acetone/Chl *b* ratio of 7300/1 is located at 643 nm; for neat acetone, the λ_{max} value is at 645 nm.

Transient absorption kinetics were measured at room temperature for Chl *b* in neat pyridine and acetone. Magic angle conditions (an angle of 54.7° between the polarizations of the excitation and probe beams) were used to monitor the rotation-free isotropic decays. Figure 4 shows the kinetics of the Chl *b* monomer in neat pyridine excited at 655 nm and probed at 650 nm (Figure 4A) and 665 nm (Figure 4B). Similar measurements with excitation at the Q_y band maximum and probing to the blue and to the red of the excitation wavelength were performed for Chl *b* in acetone (results not shown). In both solvents, the kinetics exhibit a fast decaying component of ∼100 fs when the transient absorption change was probed on the blue side of the Q_y band maximum. On the red side of the Q_y band, rise times with corresponding fast time constants were obtained. A three-component analysis of the measured kinetics also suggests the presence of a medium lifetime component (1−3 ps) in both solvents; blue-wavelength probing resolves this component as a decay, while probing on the red side of the absorption maximum reveals a rise time. The amplitude of the fast ∼100 fs component is roughly 4-fold that of the medium component regarding both the decay and the rise components. In addition, at all probe wavelengths, a dominating long decay component is present. The lifetime of this component is at least several hundred picoseconds, but the 12 ps time window of the present experiment did not allow a more precise determination of this lifetime. Lifetimes and amplitudes of the kinetics measured for Chl *b* in neat pyridine and acetone are summarized in Table 2.

Next, isotropic kinetics were measured in 3-MP for three different pyridine/Chl *b* molar ratios from the titration series. For all of the samples, excitation and probe wavelengths were similar to those used in the neat solvents (see Table 2). An aggregation-free sample possessing a minimal amount of pyridine was obtained for a pyridine/Chl *b* molar ratio of 120/1 (low pyridine concentration). At this low pyridine concentration the bulk properties of the 3-MP solvent are basically unchanged. If solvation processes related to the bulk dielectric properties of the solvent are responsible for some of the observed dynamics, this low pyridine concentration sample is expected to reflect the situation of Chl *b* monomers in nonpolar environment. On the other hand, if the pyridine molecules, which do not take part in specific coordination, form a solvent cell around Chl *b*, the situation is expected to be more complex, and already the lowest concentrations of the polar molecules could reflect the solvation dynamics of the polar solvent. To examine the effect of increasingly higher concentrations of pyridine, samples having molar ratios of 800/1 (medium pyridine concentration) and 25 000/1 (high pyridine concentration) were studied. In the sample with medium pyridine concentration, the number of 3-MP molecules is 200-fold that of the pyridine ligand, and hence, only a small red shift of the Q_y peak position is observed relative to the peak position in low pyridine concentration sample (642 nm). In contrast, the sample with high pyridine concentration, where the molarity of pyridine is

TABLE 1: Molar Ratios and Q_y Absorption Maxima for Samples from the Titration Series of Chl *b*[a]

n(pyridine)/*n*(Chl *b*)	*n*(3-MP)/*n*(pyridine)	absorpn max (nm)	*n*(acetone)/*n*(Chl *b*)	*n*(3-MP)/*n*(acetone)	absorpn max (nm)
no pyridine	neat 3-MP	645	no acetone	neat 3-MP	645
3:1	50000:1	643	2:1	115000:1	643
15:1	10000:1	642	20:1	12500:1	644
50:1	3000:1	642	70:1	4000:1	644
75:1	2000:1	642	125:1	2200:1	644
120:1	1200:1	642	250:1	1100:1	643
245:1	620:1	642	490:1	570:1	642
610:1	250:1	643	1200:1	230:1	642
1220:1	120:1	644	2400:1	115:1	642
3650:1	40:1	646	7300:1	40:1	643
7300:1	20:1	648	19500:1	15:1	643
25000:1	6:1	650	48500:1	6:1	644
245000:1	1:2	652	250000:1	1:1	644
1220000:1	1:8	654	500000:1	1:2	645
neat pyridine	no 3-MP	655	1220000:1	1:4	645
			neat acetone	no 3-MP	645

[a]Listed are pyridine/Chl *b* and acetone/Chl *b* molar ratios and number of polar solvent molecules versus 3-methylpentane molecules in the samples.

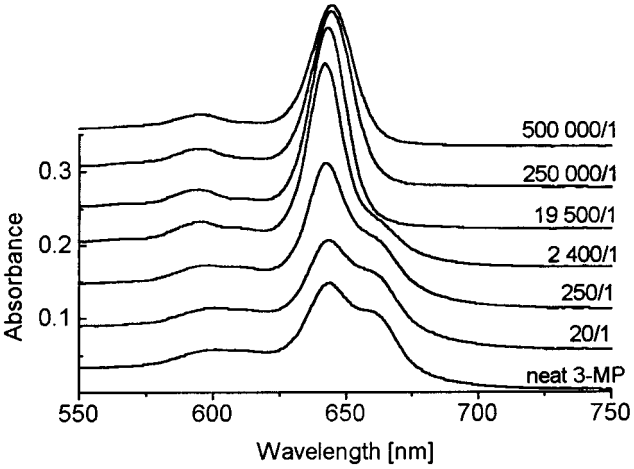

Figure 3. Titration of Chl *b* in 3-methylpentane with acetone. Molar ratios of acetone/Chl *b* for various spectra are indicated.

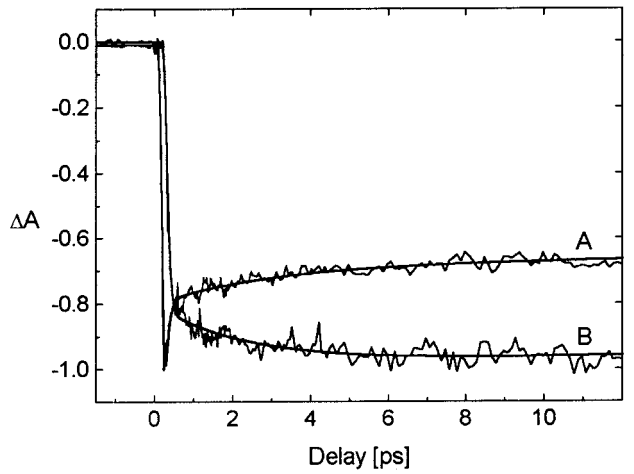

Figure 4. Isotropic kinetics of Chl *b* in neat pyridine, with 655 nm excitation; data and fits are shown. A fast decay is evident when the sample is probed at 650 nm (A) and at 665 nm (B); a fast rise is observed.

comparable to the molarity of 3-MP, shows a noticeable solvent-induced red shift of the Q_y peak to 650 nm.

All three Chl *b* samples of the 3-MP/pyridine titration series possess very similar transient absorption kinetics, characterized by three decay components ~100 fs, 1−3 ps, and >400 ps. The fast ~100 fs component is characterized by a decay on the blue side and a corresponding rise time on the red side of the PB/SE maximum. In the titration series the relative amplitude of the fast component decreases slightly with increasing pyridine concentration. Like the fast component, the medium 1−3 ps component appears as a decay on the blue side of the PB/SE maximum and grows in with a similar rise time on the red side. This component shows a more pronounced variation of the amplitude, especially in the decay on the blue side of the main PB/SE band, where there is a 3-fold increase of the amplitude in going from low-pyridine solution to neat pyridine (see Table 2). Despite the small decay amplitude of the 1−3 ps component, the ±15% amplitude error of the fitting procedure implies that the observed 3-fold amplitude increase is well outside this error. The rise on the red side does not show the same pronounced variation with pyridine concentration, mainly because of difficulties to accurately resolve the amplitude of a fast rise time component in the presence of another fast rise time (the ~100 fs component). The very slow decay component is present throughout the concentration range of the titration series with a dominating amplitude. With our short observation window of 12 ps, the lifetime of this slow component is determined only approximately.

To examine the origin of the picosecond and subpicosecond kinetic components in more detail, we measured the temporal evolution of the ΔA spectrum of Chl *b* in neat pyridine. Transient absorption spectra measured at several delay times (−50 fs to 10 ps) with different excitation wavelengths are shown in Figure 5. To avoid artifacts due to scattered light, the scattered light spectrum was measured 15 ps before the excitation, when no transient absorption signal is present, and the background-free transient absorption spectrum was obtained by subtracting the scattered light spectrum from the measured spectrum. Figure 5A shows the temporal evolution of the transient absorption spectrum, when the sample was excited at 652 nm, close to the absorption maximum. The zero-time spectrum exhibits a PB/SE maximum at 657 nm, which red shifts to 659 nm in the 10 ps spectrum. The overall temporal evolution of the time-resolved spectrum can be divided into two steps. During the first 100 fs the spectrum broadens significantly on both sides of the excitation wavelength, and after 100 fs, the main PB/SE band gradually red shifts, reaching an equilibrium position before 10 ps. With an excitation wavelength at the blue side of the absorption maximum at 645 nm, the zero-time spectrum is further shifted to the blue (λ_{max} = 652 nm), and the early-time (0−200 fs) temporal evolution is

TABLE 2: Optimized Parameters of Three-Component Fits to Two-Color Isotropic Kinetics for Chl *b* in Neat Solvents and for Three Chl *b* Samples from the Titration Series[a,b]

solvent	λ(pump)/λ(probe), nm	τ_1, fs (A_1, %)	τ_2, ps (A_2, %)	τ_3, ps (A_3, %)
neat pyridine	655/650	120 (36)	3.0 (9)	>400 (55)
neat pyridine	655/665	70 (−78)	1.1 (−22)	>400 (100)
neat acetone	645/640	100 (35)	1.7 (12)	>400 (55)
neat acetone	645/660	170 (−79)	3.2 (−21)	>400 (100)
low pyridine concn[c]	642/634	50 (49)	1.8 (3)	>400 (48)
low pyridine concn	642/654	50 (−84)	1.0 (−16)	>400 (100)
medium pyridine concn[d]	643/635	50 (47)	1.1 (5)	>400 (48)
medium pyridine concn	643/655	50 (−82)	1.3 (−18)	>400 (100)
high pyridine concn[e]	650/642	70 (46)	1.7 (7)	>400 (47)
high pyridine concn	650/662	80 (−80)	1.6 (−20)	>400 (100)

[a] Positive and negative amplitudes correspond to decay and rise components, respectively. [b]Error in femtosecond lifetime components is ±20 fs; in picosecond components it is ±10%. Amplitude error is ±15%. [c] Pyridine/Chl *b* molar ratio 120/1. [d] Pyridine/Chl *b* molar ratio 800/1. [e] Pyridine/Chl *b* molar ratio 25000/1.

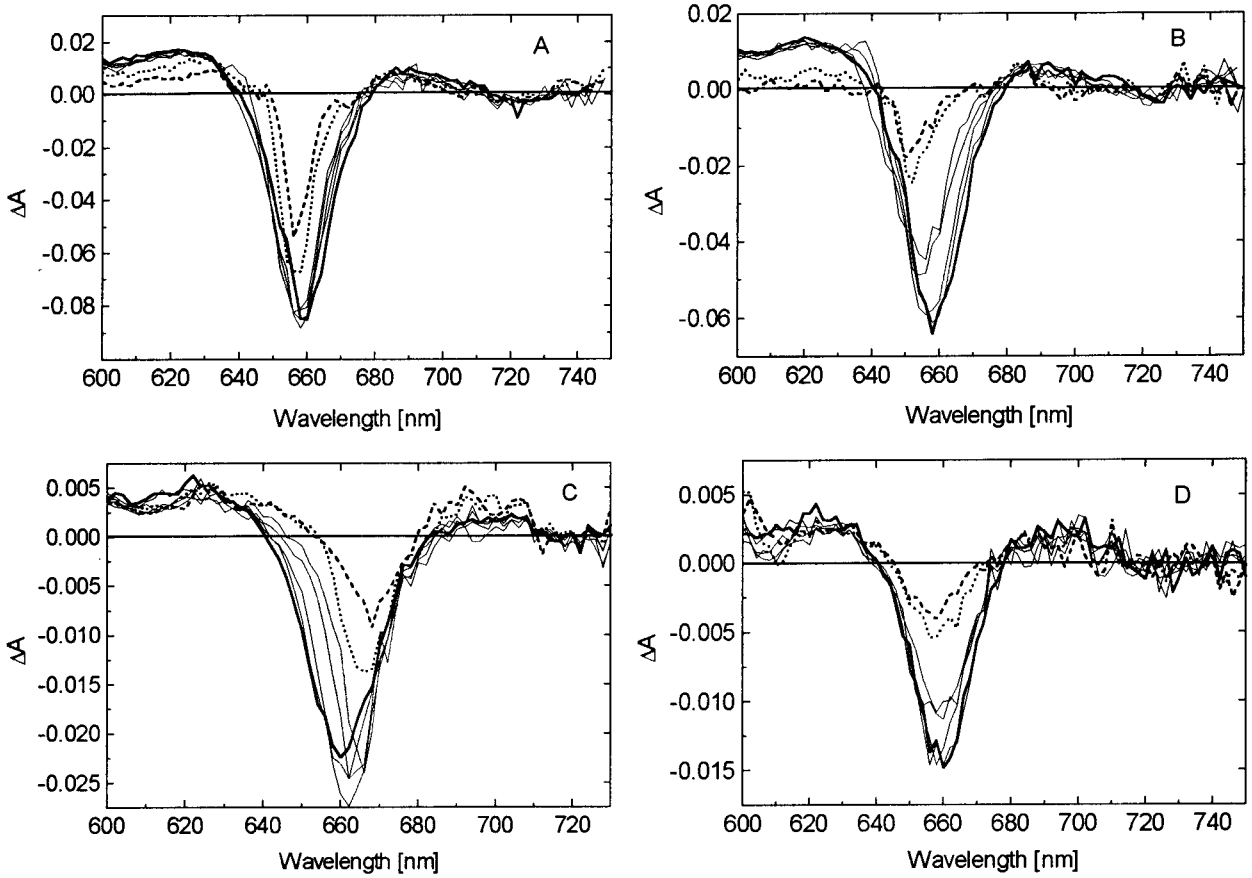

Figure 5. Temporal evolution of the Chl *b* transient absorption spectrum in neat pyridine with excitation at 652 nm (A), 645 nm (B), 670 nm (C), and 602 nm (D). Dashed spectra (---) are the spectra measured −50 fs before zero delay time, dotted spectra (···) are the $t = 0$ spectra, and thin solid lines (—) are the spectra recorded at delay times 50 fs, 100 fs, 200 fs, and 1 ps. Thick solid line (■) is the spectrum measured at 10 ps time delay.

again seen as a spectral broadening around the excitation wavelength and a red shift (Figure 5B). After 200 fs, the time-resolved spectrum has reached a shape and position very similar to that of the 200 fs spectrum with excitation at 652 nm, and only some minor further evolution occurs up to 10 ps. When the excitation wavelength is to the red of the ground-state absorption maximum at 670 nm, a red-shifted zero-time spectrum ($\lambda_{max} = 668$ nm) is observed; again the time evolution is a broadening of the spectrum, and in this case a blue-shift to the long time spectrum is observed (Figure 5C). This behavior of a correlation between excitation wavelength and the position of the early-time bleaching spectrum, as well as the ensuing spectral broadening and shift toward the equilibrated spectrum, is characteristic of a transient hole burning effect.[23] When nonselective excitation of Chl *b* into the higher lying Q_y vibronic band and Q_x band at 602 nm is used, the hole-burning effect is absent (Figure 5D), and the ΔA spectrum displays in this case very little evolution.

The transient absorption anisotropy spectrum at ∼100 fs (Figure 6A) was obtained for the sample with a pyridine/Chl *b* ratio of 800/1 by measuring the ΔA spectra with the probe beam polarized parallel and perpendicular to the excitation beam and by applying the equation

$$r_1(\lambda) = \frac{I_{||}(\lambda) - I_{\perp}(\lambda)}{I_{||}(\lambda) + 2I_{\perp}(\lambda)} \quad (1)$$

Here $r_1(\lambda)$ denotes the wavelength-dependent anisotropy at ∼100 fs delay time, and the functions $I_{||}(\lambda)$ and $I_{\perp}(\lambda)$ are the wavelength-dependent intensities of the parallel and perpen-

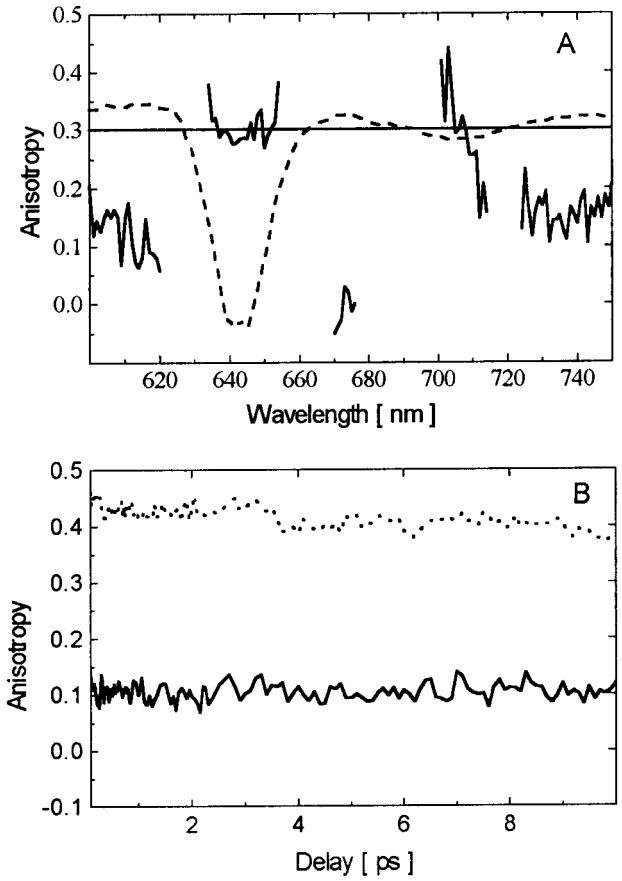

Figure 6. (A) Transient absorption anisotropy spectrum (—) of the Chl *b* sample with a pyridine/Chl *b* molar ratio of 800/1 in 3-methylpentane. The spectrum is calculated from eq 1 using parallel and perpendicular ΔA spectra measured at 100 fs delay time. Also shown is the 100 fs delay time isotropic spectrum (---). Horizontal line represents the zero level of the isotropic spectrum. The anisotropy spectrum close to isosbestic points of the isotropic spectrum is not plotted due to low signal at these wavelengths. (B) Decays of anisotropy at two probing wavelengths for the medium pyridine concentration sample measured at 655 nm (dotted line) and at 610 nm (solid line) showing initial anisotropies in good agreement with the transient absorption anisotropy spectrum in (A).

dicularly polarized transient absorption spectra, measured at a delay of ~100 fs. In a polarized transient absorption experiment involving only one optical transition, the anisotropy of the PB/SE generally varies between the limits $-0.2 \le r \le 0.4$. When probing the same transition as is excited, before possible pigment−pigment energy transfer or rotational motion of the pigment molecule occurs, an initial anisotropy value of 0.4 should be observed. The presence of ESA may considerably affect the anisotropy values; certain orientations of the ESA transition moments may yield an initial anisotropy even higher than 0.4. The Chl *b* transient absorption anisotropy spectrum shows strong variation of the initial anisotropy as a function of the wavelength. Close to the isosbestic points of the isotropic spectrum (Figure 6A), where PB/SE and ESA signals almost cancel, the measured signal is very low, leading to a noisy and meaningless anisotropy spectrum. Thus, the anisotropy values in the close vicinity of isosbestic points are not plotted. On the blue side of the spectrum (600−630 nm), ESA dominates and the anisotropy values are low (~0.1). In the range 630−665 nm in the main PB/SE band, high values of anisotropy are recorded (0.3−0.4). In a narrow range around 670 nm, the anisotropy is again low but rises to values close to 0.5 at 700 nm. At longer wavelengths (>720 nm), the anisotropy rapidly

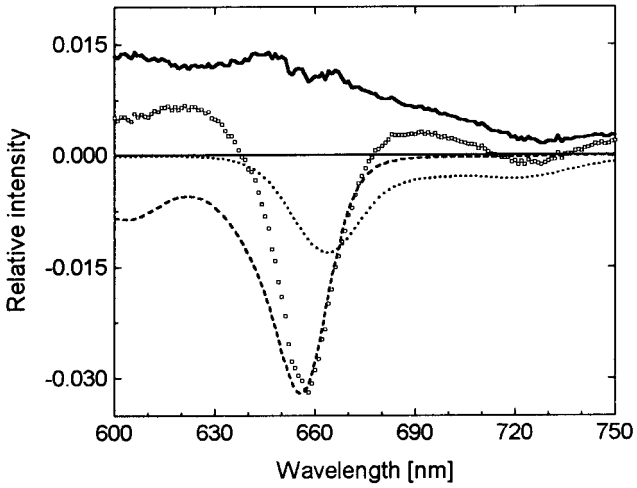

Figure 7. Simulation of Chl *b* excited-state absorption spectrum in neat pyridine (■). Shown are contributions from photobleaching (---) and stimulated emission (···). Spectrum represented by open circles (○) is the transient absorption spectrum measured at 10 ps delay time.

drops, reaching a rather constant and wavelength-independent value of 0.15. To test the reliability of the anisotropy spectrum, we measured the time-resolved decays of anisotropy at several wavelengths; Figure 6B shows the result of these measurements at two wavelengths, 655 and 610 nm. The initial anisotropies obtained from the decays were identical to those obtained from the anisotropy spectrum.

To obtain the excited-state absorption spectrum of Chl *b* in neat pyridine (Figure 7), the transient absorption spectrum was measured at 10 ps time delay and combined with the steady-state absorption spectrum and the spectrum of the stimulated emission. The latter was obtained from the spontaneous fluorescence spectrum according to the procedure given by Becker et al.[24] (eq 15). The measured ΔA spectrum is composed of bleaching of the steady-state absorption (λ_{max} at 655 nm), SE (λ_{max} at 663 nm), and excited-state absorption. The negative part of the spectrum arises from prevailing PB/SE over ESA, while the positive signal is due to prevailing ESA. The ESA spectrum [$I_{ESA}(\lambda)$] can be obtained from

$$I_{ESA}(\lambda) = I_{TA}(\lambda) - I_{PB}(\lambda) - I_{SE}(\lambda) \qquad (2)$$

where the functions are the wavelength-dependent intensities of the transient absorption [$I_{TA}(\lambda)$], photobleaching [$I_{PB}(\lambda)$], and stimulated emission [$I_{SE}(\lambda)$] spectra (Figure 7). The simulation yields the ESA spectrum to be broad and smooth over the whole wavelength range studied. For the simulation, the starting values of the relative intensities of various components were taken from the simulation of the ESA band of bacteriochlorophyll *a* (BChl *a*) in methanol, being 1.0, 0.4, and 0.6 for PB, SE, and ESA at the absorption maximum, respectively.[24] The final values of the corresponding relative intensities in our experiments of Chl *b* in pyridine are 1.0, 0.3, and 0.4 at the absorption maximum. The smoothness of the ESA spectrum was a criterion for the quality of the simulation. Even small deviations from the obtained relative intensities result in noticeable dips and bumps in the simulated ESA spectrum, giving the error limits of ±10% for the relative intensities. The difference between the relative intensities of PB and SE may originate from anharmonicity and structural differences between the ground- and excited-state potential surfaces. However, as mentioned above, the ΔA spectrum used for the calculation of the ESA spectrum was measured at 10 ps delay time. It is probable that at this time the SE part of the ΔA spectrum has not yet attained the relaxed

SE spectrum due to some slow component in solvation dynamics. This may result in large error (±30%) in the relative intensities shown in Figure 7. Nevertheless, we are quite confident that our spectra have the correct overall shape. The ESA is strongest at short wavelengths and gradually decreases toward longer wavelengths. Despite the decreasing ESA on the red side of the transient absorption spectrum, ESA never reaches the zero level in the spectral region of our study (600−750 nm) and is the major contribution to the ΔA spectrum at wavelengths above 680 nm.

On the basis of the ESA simulation, we calculated the angle between the ground-state transition moment μ_{PB} and the ESA transition moment μ_{ESA} at five wavelengths, according to the equation given by Savikhin et al.[25]

$$r(0) = \frac{2(\sigma_{PB} + \sigma_{SE}) + \sigma_{ESA}(1 - 3\theta^2)}{5(\sigma_{PB} + \sigma_{SE} - \sigma_{ESA})} \qquad (3)$$

where σ_{PB}, σ_{SE}, and σ_{ESA} are the relative intensities for PB, SE, and ESA at some distinct wavelength. The relative intensities are obtained from the simulation of the ESA spectrum, the initial anisotropy $r(0)$ is determined from the anisotropy decay of Chl *b* in neat pyridine at the required wavelength (not shown), and the angle θ denotes the angle between μ_{PB} and μ_{ESA}. In the calculation, it is assumed that the Q_y transition moments for PB and SE are parallel. The angle θ was determined for the five probe wavelengths 620, 650, 665, 700, and 720 nm to be 70°, 52°, 53°, 79°, and 67°, respectively, with an error of ±3°, indicating strong inhomogeneity of the ESA band.

Discussion

The titration experiments of Chl *b* in 3-MP show clear changes in the absorption spectrum: disappearance of the red-shifted shoulder and red shift of the main band after strongly polar (nucleophilic) molecules are added to the sample. The ligation of pyridine or acetone to the electrophilic magnesium atom of Chl *b* breaks up the self-aggregated Chl *b* and produces monomers. A red shift in the position of the Q_y band of the Chl *b* monomer is observed in the titration experiments with pyridine or acetone. The shift appears to be correlated to changes in the bulk physical properties (dipole strength, polarizability, etc.) of the solvent when the concentration of polar molecules increases in the nonpolar solvent. The solvent-induced shift is more pronounced for Chl *b* titrated with pyridine. The Q_y band red shift between the two extremes of pyridine concentration is 13 nm. For acetone, the shift is 3 nm.

A change of the coordination state of the central magnesium atom of BChl *a* has mainly an influence on the position of the Q_x absorption band,[26] but the Q_x band of Chl *b* is not well separated from the strongly absorbing Q_y region and coordination changes are therefore not straightforwardly identified in our samples from the spectral shift of the absorption spectrum. Acetone is reported to yield 5-coordinated species only. The low pyridine concentrations favor 5-coordinated Chl *b*, and in higher pyridine concentrations, essentially all of the Chl *b* is 6-coordinated.[26] In our titration experiments of Chl *b* with pyridine, we cannot observe any pronounced changes in the transient absorption kinetics that could be ascribed to possible differencies in coordination number between low and high pyridine concentrations. In addition, in neat solvents, the transient absorption kinetics are also very similar, although Chl *b* is 5-coordinated in acetone and 6-coordinated in pyridine. This shows that changes in the spectral properties and excited-state dynamics of monomeric Chl *b* in the studied solvents are essentially insensitive to the coordination number of the Mg atom of Chl *b*, and the observed variations are therefore concluded to be mainly due to changes in solvent properties.

Next, we discuss the influence of ESA on the measured anisotropy. The transient absorption spectra of Chl *b* monomers show strong ESA in the spectral region of 600−750 nm in all samples. The time window of our measurements (0−12 ps) and the Chl *b* concentration used (5×10^{-5} mol/L) ensure that depolarizing pigment−pigment energy transfer and rotational relaxation do not contribute significantly to anisotropy values. This is because the rotational correlation times of chlorophylls in low-viscosity solvents are on the order of hundreds of picoseconds, and at the low Chl *b* concentrations used, average Chl *b*−Chl *b* distances in the solution are large enough to make energy transfer very slow.[18,27] For a two-level system, possessing a ground and an excited state and collinear transition moments of PB and SE, the initial anisotropy at $t = 0$ should be 0.4. Under these conditions, strong ESA, indicating the presence of higher excited states, may violate the picture. Thus, the interplay of PB/SE and ESA may yield unexpected anisotropy values, and in this case, the observed anisotropy depends on the direction of the ESA transition moment and the ESA cross section.[28]

On the blue side (600−630 nm) of the transient absorption spectrum, low anisotropy values are obtained. Strong ESA governs this part of the spectrum, since the cross section for PB/SE is small. The main PB/SE band (635−655 nm) has high anisotropy, because the cross section of PB/SE is high in this region. Nevertheless, the anisotropy does not reach the maximum value 0.4 due to the ESA that also contributes to the absorption signal at the maximum of the PB/SE band. At 670−680 nm, anisotropy is again low. The isotropic transient absorption spectrum shows a positive signal in this region, suggesting that in this wavelength region the cross section of ESA is higher than that of SE. At ∼700 nm, the ΔA spectrum is dominated by a vibrational band of the SE, and since ESA is low, this leads to high anisotropy values. Above 700 nm, the anisotropy drops down to a value of 0.15 and remains constant at all longer wavelengths, the influence of ESA being dominant at these red wavelengths.

As was described in the Results section, the ESA spectrum for Chl *b* in neat pyridine was obtained from the measured ΔA spectrum and the absorption and fluorescence spectra. The broad and featureless ESA band spans over the whole spectral region of 600−750 nm. The question arises whether the ESA band represents only one transition to a higher excited state or whether it is composed of several transitions to higher excited states. If the measured ESA transitions were spectroscopically allowed in the ground-state absorption spectrum, they would appear in the wavelength range 310−350 nm. On the basis of the calculated angles between PB and ESA transition moments, it is obvious that several ESA transitions contribute in the spectral region of our study (600−750 nm). Within the experimental errors, the two probe wavelengths at 650 and 665 nm represent the same ESA transition, because the obtained angles between μ_{PB} and μ_{ESA} are practically the same (52° and 53°). Correspondingly, large differences in the calculated angles at the other three analyzing wavelengths suggest that the three wavelengths represent different transitions to higher excited states. Therefore, our results indicate that $S_1 \rightarrow S_n$ ESA has a contribution from at least four different higher excited states in the wavelength region 600−750 nm.

Now we turn to a discussion of the temporal evolution of the ΔA spectrum. By comparing kinetics measured at different wavelengths (Figure 4) with the ΔA spectra measured at different delay times (Figure 5), it is evident that the ∼100 fs time constant is related to the spectral broadening and shifting following excitation with the ∼100 fs pulses. If excitation is in the blue wing of the ground-state absorption spectrum (Figure 5B), the time-resolved ΔA spectrum rapidly red shifts and broadens toward the long-time (steady-state) spectrum. On the other hand, if the sample is excited in the red wing of the absorption spectrum (Figure 5C), the time-resolved spectrum blue shifts toward the long-time spectrum as it acquires the shape of the spectrum at long times. Thus, the initial ΔA spectrum at $t = 0$ is correlated to the center wavelength of the excitation pulse and shifts very rapidly on the few 100 fs time scale to the long-time (10 ps) spectrum. This leads to a rapid (∼100 fs) decay in kinetics measured at blue wavelengths and a corresponding fast rise time in kinetics measured in the red wing of the ΔA spectrum (Figure 4). This behavior shows characteristics of transient spectral hole burning of the inhomogeneously broadened ground-state absorption spectrum, following excitation with a ∼100 fs laser pulse having a spectral width of 300 cm^{-1}. Brito Cruz et al.[23] have observed similar time-dependent hole burning and equilibration to a thermalized population distribution to occur within ∼100 fs for cresyl violet in ethylene glycol. In the case of Chl *b* in neat pyridine, the solute−solvent interactions induce the inhomogeneity of the absorption spectrum. At room temperature, when fluctuations of solute−solvent interactions (dephasing processes) occur on the tens of femtoseconds time scale, the spectral hole filling will be very fast as observed in the experiments. The ultrafast dynamics of an optically excited molecule may originate from several different processes and interactions.[29] In addition to the transient spectral hole burning discussed above, intermolecular vibrational redistribution and vibrational cooling may contribute to the dynamics as was suggested by Savikhin et al. for BChl *a* in 1-propanol.[25]

When vibrational relaxation in chlorophyll-like large pigment molecules takes place, changes in the shape of the PB/SE spectrum are expected to occur, and the changes should in the experiment mainly be observed as a temporal narrowing of the PB/SE spectrum.[30,31] In our time-resolved measurements of Chl *b* in pyridine, no spectral narrowing is observed at delay times longer than 200 fs, and therefore we believe that vibrational relaxation in the first excited state occurs within 200 fs, simultaneously with the ground-state hole-filling process. Quite short vibrational relaxation times (<70 fs) have been recently reported for other large polyatomic molecules.[31,32] Due to the strong contribution of ground-state hole filling to the early time evolution of the transient absorption spectra (0−200 fs), it is not possible to gain more detailed knowledge of vibrational relaxation from the present experiments.

We assign the 1−3 ps component to solvation dynamics, the response of the surrounding solvent to the photoexcitation of the Chl *b* molecule, to achieve minimum solvation energy. In the transient absorption spectra, the solvent relaxation is observed as a temporal red shift of the SE contribution. Using this approach, the effect of adding more pyridine to the 3-MP solution in the titration series will be to increase the overall dielectric response of the bulk solvent, since pyridine is a polar solvent (dielectric constant 12.3) and 3-MP is a nonpolar solvent. This is expected to lead to an increased contribution from the solvent component (the 1−3 ps lifetime) to the Chl *b* kinetics, in good agreement with the results of our measurements (compare Table 2). The fact that a substantial amplitude of the 1−3 ps solvation component is present already in the lowest pyridine concentration (see Table 2) suggests that there is preferential solvation of Chl *b* by the pyridine molecules in the pyridine/3-MP solutions. Transient absorption kinetics of BChl *a* monomers in pyridine[24] and methanol[33] revealed similar time constants (2−3 ps) which also were assigned to dielectric relaxation of the solvent. Further we assign the long (>400 ps) lifetime component that is present in all kinetic traces to the lifetime of the first excited state of the Chl *b* monomer. In acetonitrile and benzene, the Chl *b* fluorescence lifetime has been reported to be 2.5 and 6.3 ns, respectively.[34,35]

Conclusions

A time-resolved transient absorption study of Chl *b* monomers in the neat polar solvents pyridine and acetone was presented. Chl *b* monomers were also prepared in 3-methylpentane by adding pyridine to the sample to yield different pyridine/Chl *b* molar ratios. The excited-state absorption of Chl *b* was observed to be very strong in the wavelength range of our study (600−750 nm) and to alter significantly the measured anisotropy values. From the simulation of the excited-state absorption spectrum, we observed that several higher excited states are present in the range 600−750 nm, resulting in a broad and smooth excited-state absorption spectrum. In the time-resolved measurements, two fast lifetime components (∼100 fs and 1−3 ps) were observed in all samples, and the amplitude of the latter component was sensitive to changes in the solvent environment, suggesting the 1−3 ps component to be connected to solvent relaxation. The ∼100 fs component was interpreted as that arise from transient spectral hole burning of the ground-state absorption spectrum.

Acknowledgment. J.A.I. Oksanen is grateful to NorFA and Lund Laser Centre for support of this study (Contract ERBFMGECT950020(DG12)). Support of this work was also provided from Crafoordska Stiftelsen, Magn. Bergvalls Stiftelse, the Swedish Natural Science Research Council, and the Knut and Allice Wallenberg Foundation.

References and Notes

(1) van Grondelle, R.; Dekker, J. P.; Gillbro, T.; Sundström, V. *Biochim. Biophys. Acta* **1994**, *1187*, 1.

(2) Sundström, V.; van Grondelle, R. *Anoxygenic Photosynthetic Bacteria*; Kluwer Academic Publishers: Dordrecht, The Netherlands, 1995; Chapter 17.

(3) Kühlbrandt, W.; Wang, D. N.; Fujiyoshi, Y. *Nature* **1994,** *367*, 614.

(4) Seely, G. R.; Jensen, R. G. *Spectrochim. Acta* **1965,** *21*, 1835.

(5) Hynninen, P. H.; Lötjönen. S. *Synthesis* **1983,** *9*, 705.

(6) Eads, D. D.; Castner Jr., E. W.; Alberte, R. S.; Mets, L.; Fleming, G. R. *J. Chem. Phys.* **1989**, *93*, 8271.

(7) Du, M.; Xie, X.; Mets, L.; Fleming, G. R. *J. Phys. Chem.* **1994**, *98*, 4736.

(8) Bittner, T.; Irrgang, K.-D.; Renger, G.; Wasielewski, M. R. *J. Phys. Chem.* **1994**, *98*, 11821.

(9) Bittner, T.; Wiederrecht, G. P.; Irrgang, K.-D.; Renger, G.; Wasielewski, M. R. *Chem. Phys.* **1995**, *194*, 311.

(10) Visser, H. M.; Kleima, F. J.; van Stokkum, I. H. M.; van Grondelle, R.; van Amerongen, H. *Chem. Phys.* **1996**, *210*, 297.

(11) Pålsson, L.-O.; Spangfort, M. D.; Gulbinas, V.; Gillbro, T. *FEBS Lett.* **1994,** *339*, 134.

(12) Kwa, S. L. S.; van Amerongen, H.; Lin, S.; Dekker, J. P.; van Grondelle, R.; Struve, W. S. *Biochim. Biophys. Acta* **1992**, *1102*, 202.

(13) Savikhin, S.; van Amerongen, H.; Kwa, S. L. S.; van Grondelle, R.; Struve, W. S. *Biophys. J.* **1994,** *66*, 1597.

(14) Gillbro, T.; Sundström, V.; Sandström, Å.; Spangfort, M.; Andersson, B. *FEBS Lett.* **1985**, *193*, 267.

(15) Hynninen, P. *Acta Chem. Scand.* **1977**, *B31*, 829.

(16) Hynninen, P. H.; Wasielewski, M. R.; Katz, J. J. *Acta Chem. Scand.* **1979**, *B33*, 637.

(17) Chachisvilis, M. Electronic and vibrational coherence in photosynthetic and model systems. Thesis, Lund University, 1996; p 26.

(18) Helenius, V. M.; Hynninen, P. H.; Korppi-Tommola, J. E. I. *Photochem. Photobiol.* **1993**, *58*, 867.

(19) Ballschmiter, K.; Truesdell, K.; Katz, J. J. *Biochim. Biophys. Acta* **1969**, *184*, 604.

(20) Oksanen, J. A. I.; Helenius, V. M.; Hynninen, P. H.; van Amerongen, H.; Korppi-Tommola, J. E. I.; van Grondelle, R. *Photochem. Photobiol.* **1996**, *64*, 356.

(21) Cotton, T. M.; Loach, P. A.; Katz, J. J.; Ballschmiter, K. *Photochem. Photobiol.* **1978**, *27*, 735.

(22) Katz, J. J.; Shipman, L. L.; Cotton, T. M.; Janson, T. R. *The Porphyrins;* Academic Press: New York, 1978; Vol. V, p 401.

(23) Brito Cruz, C. H.; Fork, R. L.; Knox, W. H.; Shank, C. V. *Chem. Phys. Lett.* **1986**, *132*, 341.

(24) Becker, M.; Nagarajan, V.; Parson, W. W. *J. Am. Chem. Soc.* **1991**, *113*, 6840.

(25) Savikhin, S.; Struve, W. S. *Biophys. J.* **1994**, *67*, 2002.

(26) Evans, T. A.; Katz, J. J. *Biochim. Biophys. Acta* **1975**, *396*, 414.

(27) Myslinski, P.; Koningstein, J. A. *Chem. Phys.* **1992**, *161*, 273.

(28) Hess, S.; Feldchtein, F.; Babin, A.; Nurgaleev, I.; Pullerits, T.; Sergeev, A.; Sundström, V. *Chem. Phys. Lett.* **1993**, *216*, 247.

(29) Cho, M.; Yu, J. Y.; Joo, T.; Nagasawa, Y.; Passino, S. A.; Fleming, G. R. *J. Phys. Chem.* **1996**, *100*, 11944.

(30) Struve, W. S. *Biophys. J.* **1995**, *69*, 2739.

(31) Horng, M. L.; Gardecki, J. A.; Papazyan, A.; Maroncelli, M. *J. Phys. Chem.* **1995**, *99*, 17311.

(32) Kovalenko, S. A.; Ernsting, N. P.; Ruthmann, J. *J. Chem. Phys.* **1997**, *106*, 3504.

(33) Hess, S.; Åkesson, E.; Cogdell, R. J.; Pullerits, T.; Sundström, V. *Biophys. J.* **1995**, *69*, 2211.

(34) Dsmagarov, B. M.; Sagun, E. Y.; Gamska, V. A.; Gurikovich, G. P. *Chim. Fiz.* **1987**, 919.

(35) Brody, S. S.; Rabinowitch, E. *Science* **1957**, *125*, 55